

End-to-End Learning for Integrated Sensing and Communication

José Miguel Mateos-Ramos*, Jinxiang Song*, Yibo Wu*[†], Christian Häger*,
Musa Furkan Keskin*, Vijaya Yajnanarayana[‡], Henk Wymeersch*

*Department of Electrical Engineering, Chalmers University of Technology, Sweden

[†]Ericsson Research, Sweden, [‡]Ericsson Research, India

Abstract—Integrated sensing and communication (ISAC) aims to unify radar and communication systems through a combination of joint hardware, joint waveforms, joint signal design, and joint signal processing. At high carrier frequencies, where ISAC is expected to play a major role, joint designs are challenging due to several hardware limitations. Model-based approaches, while powerful and flexible, are inherently limited by how well the models represent reality. Under model deficit, data-driven methods can provide robust ISAC performance. We present a novel approach for data-driven ISAC using an auto-encoder (AE) structure. The approach includes the proposal of the AE architecture, a novel ISAC loss function, and the training procedure. Numerical results demonstrate the power of the proposed AE, in particular under hardware impairments.

Index Terms—Integrated sensing and communication, Joint radar and communications, Auto-encoder, Machine learning.

I. INTRODUCTION

Progressive generations of mobile communication systems have moved up in carrier frequency to unlock ever larger bandwidths, starting with 5G in the mmWave band and 6G envisioned to operate above 100 GHz [1]–[3]. The combination of large bandwidths and large arrays is reminiscent of high-resolution radar, available, e.g., to support autonomous driving (AD) and advanced driver-assistance system (ADAS) applications in modern vehicles [4]. This observation has led to the introduction of integrated sensing and communication (ISAC), where the same spectrum is used for both radar-like sensing and high-rate communication [5]–[9].

According to [7], ISAC’s history can be traced back in the radar community to the 1960s, an example of which is the missile range instrumentation radar [10]. In the communication community, ISAC has only recently found traction, after the introduction of orthogonal frequency-division multiplexing (OFDM) radar [11]. Unlike pulsed or continuous wave radars, OFDM radars are resilient to wireless channels due to the inherent frequency diversity which enhances the sensing performance [12]. ISAC systems can be developed in a number of ways, including (approximately) orthogonal designs (in time [13], [14], frequency [15], or space [16], [17]) and joint waveforms (referred to as unified designs in [7, Table III]). Joint waveforms are attractive from an efficiency point of view in monostatic¹ sensing, as the entire communication signal can

be used for radar sensing and vice versa.

The literature on joint waveforms for ISAC includes (i) communication waveforms used for sensing, e.g., [11], [18]; (ii) sensing waveforms used for communication, e.g., [19], [20]; and (iii) flexible designs that offer a trade-off between communication or sensing [5], [21]–[29]. Existing approaches in the latter category differ in terms of the *ISAC objective function* (e.g., radar and communication information rates [5], weighted radar peak-to-sidelobe level and communication signal-to-noise ratio (SNR) [21], transmit power with interference constraints [22], radar SNR under communication similarity constraint [23], generalized radar metrics under communication error constraints [24], communication interference subject to a communication similarity constraint [25], radar Cramér-Rao bound (CRB) under rate constraints [26], communication rate under CRB [27] and radar similarity [29] constraints) and the *ISAC optimization variables* (e.g., power [5], [29], signal covariance [21], beamformers [22], [24], [26], [27], transmit sequences across antennas [23], [25], weighted multibeams [28]).

Since the optimization problem in joint waveform design is often non-convex, approximate solution techniques are often applied, including those based on machine learning (ML) [27]. Data-driven ML methods are also useful under model deficits, e.g., to mitigate effects of array calibration errors, mutual coupling, power amplifier nonlinearity, quantization effects etc., which are expected to be prevalent in 6G [9]. Hence, ML-based designs are a promising alternative to conventional model-based approaches (see, e.g., [30], [31]). In particular, end-to-end autoencoders (AEs) [32] are potentially well-suited for ISAC problems because they allow for the joint optimization of both the transmit waveforms as well as the communication and radar receivers. While AEs have been widely applied for communication [33]–[36] and radar [37]–[39] systems separately, AE-based designs have not been investigated in the ISAC literature.

In this paper, we propose a novel AE tailored to ISAC. We study a simplified single-target narrowband setting and generalize existing studies on end-to-end AE communication to the ISAC setting. Our specific contributions are as follows: (i) a novel AE architecture to perform joint sensing and communication; (ii) a novel loss function for radar sensing accounting for both target detection, target regression, and uncertainty quantification, which is subsequently combined

¹The ISAC literature has mainly focused on monostatic sensing, since for bistatic or multistatic sensing a pilot signal is transmitted. Hence, waveform design problems are different than in the monostatic case.

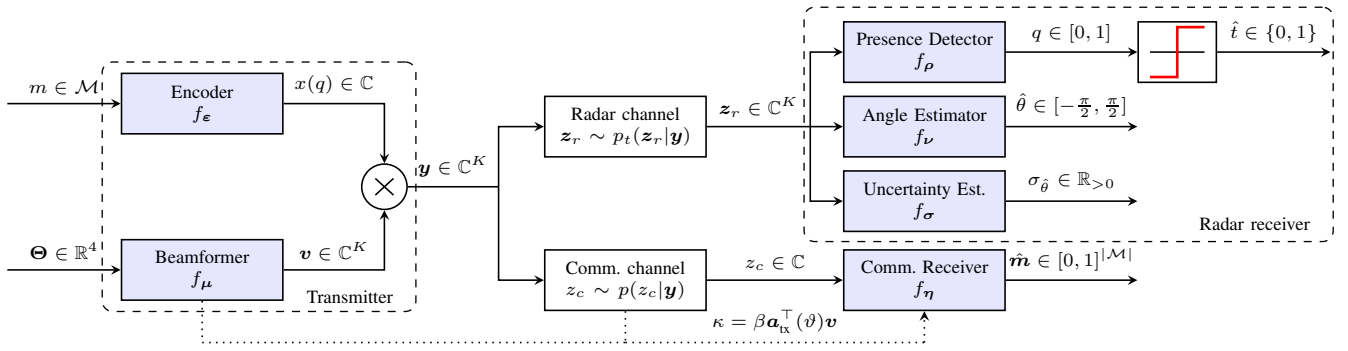


Fig. 1: Block diagram of the ISAC system model. The blocks highlighted in blue are implemented as trainable NNs as part of the proposed AE. The radar receiver is assumed to be co-located with the transmitter, while the communication receiver is remote.

with the standard communication categorical cross-entropy (CCE) loss; (iii) a detailed performance comparison to the best known benchmarks, indicating similar performance; (iv) a case study in the presence of hardware impairments, demonstrating the robustness of the proposed AE over the model-based benchmarks.

II. SYSTEM MODEL

A block diagram of the considered system model is shown in Fig. 1. In the following, we first look at the radar and communication systems separately and then describe the model to perform the joint task of radar sensing and communication.

A. Single-target MIMO Radar

We consider a multi-input multi-output (MIMO) radar transceiver, which sends a complex signal $\mathbf{y} \in \mathbb{C}^K$ across K antennas, subject to $\mathbb{E}\{\|\mathbf{y}\|^2\} \leq E_{\text{tx}}$. At the co-located radar receiver, a signal $\mathbf{z}_r \sim p_t(\mathbf{z}_r|\mathbf{y})$ across the K receive antennas is observed, where $t \in \{0, 1\}$ represents the absence or presence of a target, with $p(t=1) = 1/2$. In the absence of a target $\mathbf{z}_r = \mathbf{n}$, while in the presence of a target

$$\mathbf{z}_r = \alpha \mathbf{a}_{\text{rx}}(\theta) \mathbf{a}_{\text{tx}}^\top(\theta) \mathbf{y} + \mathbf{n}, \quad (1)$$

where $\mathbf{n} \sim \mathcal{CN}(\mathbf{0}, N_0 \mathbf{I}_K)$ with noise power spectral density N_0 , $[\mathbf{a}_{\text{tx}}(\theta)]_k = [\mathbf{a}_{\text{rx}}(\theta)]_k = \exp(-j2\pi kd \sin(\theta)/\lambda)$, with $d = \lambda/2$. We further assume that $\alpha \sim \mathcal{CN}(0, \sigma_r^2)$, following a Swerling-1 model of the target, in which σ_r^2 captures the loss of power due to path loss and the target's radar cross section, and that the target (if present) is known to lie in a certain angle-of-arrival (AoA) interval (equivalent to the angle-of-departure (AoD) interval) $\theta \sim \mathcal{U}[\theta_{\min}, \theta_{\max}]$, with $-\pi/2 \leq \theta_{\min} \leq \theta_{\max} \leq \pi/2$.

The purpose of the radar receiver is to determine the probability $q \in [0, 1]$ that a target is present, and, if so, determine an estimate $\hat{\theta}$ of the AoA with an uncertainty estimate $\sigma_{\hat{\theta}}$.

B. MISO Communication

The transmitter sends a message $m \in \mathcal{M}$, which should be mapped onto a constellation and precoded to achieve high SNR at the receiver. We denote the transmitted signal across the K antennas by $\mathbf{y}(m) = \mathbf{v}x(m)$ (again subject to $\mathbb{E}\{\|\mathbf{y}\|^2\} \leq E_{\text{tx}}$), where $\mathbf{v} \in \mathbb{C}^K$ is the transmit beamformer and $x(m) \in \mathbb{C}$

is the mapping of the message in the in-phase/quadrature (IQ) plane. We consider a remote receiver with one antenna. The observed signal is given by

$$z_c = \beta \mathbf{a}_{\text{tx}}^\top(\vartheta) \mathbf{y}(m) + n, \quad (2)$$

where the channel is modeled as Rayleigh, with $\beta \sim \mathcal{CN}(0, \sigma_c^2)$, and the communication receiver is known to lie in a certain AoD range $\vartheta \sim \mathcal{U}[\vartheta_{\min}, \vartheta_{\max}]$, with $-\pi/2 \leq \vartheta_{\min} \leq \vartheta_{\max} \leq \pi/2$.

The purpose of the communication receiver is to recover the transmitted message m . In order to focus on the core communication functionality, we assume that a pilot sequence has been sent prior to data transmission, so that the communication receiver has access to channel state information (CSI) $\kappa = \beta \mathbf{a}_{\text{tx}}^\top(\vartheta) \mathbf{v}$ (see, e.g., [40] for ML-based CSI estimation methods).

C. Integrated Sensing and Communication

In the ISAC setting, the goal of the transmitter is to design $\mathbf{y}(m)$ as well as the corresponding radar and communication receivers to jointly optimize communication and radar performance. The transmitter has knowledge of $\Theta = [\theta_{\min}, \theta_{\max}, \vartheta_{\min}, \vartheta_{\max}]$, which accounts for the possible locations of the target and the communication receiver. Such a joint optimization must account for trade-offs between sensing and communication performance, as discussed in Section I.

Benchmark solutions for radar, communication, and ISAC are deferred to Section IV-B.

III. ISAC END-TO-END LEARNING

To solve the ISAC problem, we propose to use an end-to-end learning approach via a novel AE architecture and associated loss functions, as described in the following.

A. AE Architecture

We implement each of the six highlighted blocks in Fig. 1 as a feed-forward neural network (NN). In particular, we express the encoder and beamformer as functions $f_\epsilon: \mathcal{M} \rightarrow \mathbb{C}$ and $f_\mu: \mathbb{R}^4 \rightarrow \mathbb{C}^K$, respectively, where ϵ and μ are the learnable parameters of each network. Similarly, the presence detector $f_\rho: \mathbb{C}^K \rightarrow [0, 1]$, angle estimator $f_\nu: \mathbb{C}^K \rightarrow [-\pi/2, \pi/2]$, uncertainty estimator $f_\sigma: \mathbb{C}^K \rightarrow \mathbb{R}_{>0}$, and communication receiver $f_\eta: \mathbb{C} \rightarrow [0, 1]^{|M|}$ are a function of the learnable

parameters ρ , ν , σ , and η , respectively. The inputs and outputs to each NN are shown in Fig. 1. The radar and communication channel blocks are both instantaneously differentiable, which means that they are differentiable under a realization of the random variables linked to them. This enables supervised end-to-end learning of all NNs, with training labels $[m, t, \theta]$.

B. Loss Functions

1) *Target Detection*: The output from the detector is an estimate of the probability $q \in [0, 1]$ that the target is present. During testing, a threshold can then be applied to q . An appropriate metric for this type of estimation is the binary cross-entropy (BCE) loss, defined as

$$\mathcal{J}_{\text{TD}}(\varepsilon, \mu, \rho) = -\mathbb{E}[t \log(q) + (1 - t) \log(1 - q)], \quad (3)$$

where the expectation is over the noise, the presence/absence of a target, the radar channel gain, and the true target AoA.

2) *Target Regression*: If a target is present, a regression loss can be used to assess how well the AE determines the target's AoA. Rather than simply using the mean squared error (MSE) $\mathbb{E}[|\hat{\theta} - \theta|^2]$, which only learns the target's AoA, we propose to use the negative log-likelihood (NLL)

$$\begin{aligned} \mathcal{J}_{\text{TR}}(\varepsilon, \mu, \rho, \sigma) &= -\mathbb{E}[\log(p(\hat{\theta}|\theta))] \\ &= \mathbb{E}\left[\log(\sigma_{\hat{\theta}}) + \frac{1}{2\sigma_{\hat{\theta}}^2}|\theta - \hat{\theta}|^2\right], \end{aligned} \quad (4)$$

where we approximated the likelihood $p(\hat{\theta}|\theta)$ with a Gaussian density $\hat{\theta} \sim \mathcal{N}(\theta, \sigma_{\hat{\theta}}^2)$. Through this loss function, the receiver learns both the target's AoA $\hat{\theta}$ and the corresponding uncertainty $\sigma_{\hat{\theta}}$, which can be useful for subsequent processing.

3) *Overall Radar Loss Function*: Combining the detection and regression loss lead to a joint NLL loss, proposed in [41]

$$\mathcal{J}_{\text{NLL}}(\varepsilon, \mu, \rho, \nu, \sigma) = \mathcal{J}_{\text{TD}} + p(t = 1)\mathcal{J}_{\text{TR}}. \quad (6)$$

4) *Communication Loss Function*: We apply the widely used CCE loss. Let $C = |\mathcal{M}|$, $\mathbf{m}^{\text{enc}} \in \{0, 1\}^C$ be the one-hot encoding [32] of m and $\hat{\mathbf{m}} \in [0, 1]^C$ a C -dimensional probability vector. Then, the CCE loss is

$$\mathcal{J}_{\text{CE}}(\varepsilon, \mu, \eta) = -\mathbb{E}\left[\sum_{j=1}^C m_j^{\text{enc}} \log(\hat{m}_j)\right]. \quad (7)$$

5) *ISAC loss*: In order to combine the loss functions from the radar and communication transceivers, we consider a joint loss function as a linear combination of the individual losses

$$\mathcal{J}_{\text{ISAC}}(\varepsilon, \mu, \rho, \sigma, \nu, \eta) = \omega_r \mathcal{J}_{\text{NLL}} + (1 - \omega_r) \mathcal{J}_{\text{CE}}, \quad (8)$$

where $\omega_r \in [0, 1]$ is a hyper-parameter to trade off radar performance for communication performance.

IV. RESULTS

In this section, we describe the simulation parameters, the performance metrics, the benchmarks, and finally the simulation results with discussion. Cases without and with hardware impairments are considered.

A. Simulation Parameters and Metrics

We set $|\mathcal{M}| = 4$, $K = 16$, and $\mathbb{E}\{\|\mathbf{y}\|^2\} = 1$. The average SNR in the communication is $\text{SNR}_c = \sigma_c^2/N_0 = 20$ dB (both for training and testing). The possible receiver locations lie in the range $(\vartheta_{\min}, \vartheta_{\max}) = (30^\circ, 50^\circ)$. The average SNR in the radar model is $\text{SNR}_r = \sigma_r^2/N_0 = 0$ dB, and the target can be located in $(\theta_{\min}, \theta_{\max}) = (-20^\circ, 20^\circ)$.

To evaluate the communication performance, we use the symbol error rate (SER) $\mathbb{E}[p(\hat{m} \neq m)]$. To evaluate the radar performance, we use the detection probability $P_d = p(\hat{t} = 1|t = 1)$, false alarm probability $P_{\text{fa}} = p(\hat{t} = 1|t = 0)$, and root mean squared error (RMSE), $\sqrt{\mathbb{E}[|\hat{\theta} - \theta|^2]}$ (only when $\hat{t} = t = 1$, i.e., when a target is present and detected).

B. Benchmarks

1) *Transmitter Benchmark*: As communication constellation, we use 4-QAM. For communication and radar beamforming vector, we use the approach from [42], [43]. In particular, given an certain angular range $[\theta_{\min}, \theta_{\max}]$ (i.e., either for communication or radar), let $\mathbf{b} \in \mathbb{C}^{N_{\text{grid}} \times 1}$ denote the desired beampattern at N_{grid} angular grid locations $\{\theta_i\}_{i=1}^{N_{\text{grid}}}$, with

$$[\mathbf{b}]_i = \begin{cases} |\mathbf{a}_{\text{tx}}(\theta_i)|^2, & \text{if } \theta_i \in [\theta_{\min}, \theta_{\max}] \\ 0, & \text{otherwise} \end{cases}. \quad (9)$$

Let $\mathbf{A} = [\mathbf{a}_{\text{tx}}(\theta_1) \dots \mathbf{a}_{\text{tx}}(\theta_{N_{\text{grid}}})] \in \mathbb{C}^{K \times N_{\text{grid}}}$ the transmit steering matrix corresponding to those locations. Then, the beampattern synthesis problem can be formulated as $\min_{\mathbf{y}} \|\mathbf{b} - \mathbf{A}^T \mathbf{y}\|_2^2$, which has a simple closed-form least-squares (LS) solution $\mathbf{y} = (\mathbf{A}^* \mathbf{A}^T)^{-1} \mathbf{A}^* \mathbf{b}$. After normalization, this provides us with a communication-optimal beam \mathbf{y}_c and a radar-optimal beam \mathbf{y}_r . For the ISAC scenario, we apply the approach from [28], and design the transmit ISAC beam as

$$\mathbf{v}(\rho, \varphi) = \sqrt{E_{\text{tx}}} \frac{\sqrt{\rho} \mathbf{y}_r + \sqrt{1 - \rho} e^{j\varphi} \mathbf{y}_c}{\|\sqrt{\rho} \mathbf{y}_r + \sqrt{1 - \rho} e^{j\varphi} \mathbf{y}_c\|}. \quad (10)$$

where $\rho \in [0, 1]$ is a trade-off parameter and $\varphi \in [0, 2\pi)$ is a phase that can be used to provide coherency between multiple beams. Such a beam can then be optimized with respect to ρ, φ in terms of different objectives [14], [28]. For our purpose, it is sufficient to sweep over $[\rho, \varphi]$ and for each value evaluate the SER, RMSE, detection and false alarm probabilities for the corresponding optimized communication and radar receiver benchmarks, detailed next.

2) *Radar Detection Benchmark*: To derive a benchmark for radar detection, we resort to the maximum a-posteriori (MAP) ratio test (MAPRT) detector [44], which generalizes the generalized likelihood ratio test (GLRT) detector [45] to the case with random parameters and thus can take into account the prior information on α and θ . Details can be found in Appendix A.

TABLE I: Summary of the NN architectures.

| Network | Input layer | Hidden layers | Output layer |
|-----------------------------|-----------------|---------------|---------------------------|
| Encoder f_ε | $ \mathcal{M} $ | $(K, K, 2K)$ | 2 (linear) |
| Beamformer f_μ | 4 | $(K, K, 2K)$ | K (linear) |
| Presence det. f_ρ | $2K$ | $(2K, 2K, K)$ | 1 (sigmoid) |
| Angle est. f_ν | $2K$ | $(2K, 2K, K)$ | 1 (tanh) |
| Uncertainty est. f_σ | $2K$ | $(2K, 2K, K)$ | 1 (ReLU) |
| Comm. receiver f_η | 2 | $(K, 2K, 2K)$ | $ \mathcal{M} $ (softmax) |

3) *Communication Receiver Benchmark*: We apply the maximum likelihood detector

$$\hat{m}(z_c) = \arg \min_{m \in \mathcal{M}} \|z_c - \beta \mathbf{a}_{\text{tx}}^\top(\vartheta) \mathbf{v} x(m)\|^2, \quad (11)$$

which minimizes the SER.

C. AE Training

In terms of the NN architectures, Table I shows the size of the layers in each network, as well as the activation functions for the output layer. The activation function for the hidden layers is the Rectified Linear Unit (ReLU) function. Complex-valued inputs are converted to real-valued by concatenating their real and imaginary parts. In the transmitter, after computing \mathbf{y} , we apply a normalization layer, which scales the transmitted signal to meet the power constraint, as proposed in [32]. To train the AE, we employed the widely used Adam optimizer [46] with learning rate 0.01 and mini-batch size 10000. The data samples in each mini-batch are drawn independently from the corresponding distribution (source or channel). Thus, no data is reused between training and testing, preventing overfitting issues. We utilized a total of 20 million samples to train each NN.

Given the losses in (3)–(8), we could train all six NNs from Table I at the same time. However, we found that sequentially training the radar receiver NNs yielded better performance. We maintain the joint training structure of (8), but with slight changes to \mathcal{J}_{NLL} . Namely, we first train $f_\varepsilon, f_\mu, f_\eta, f_\nu$ substituting \mathcal{J}_{NLL} in (8) by a modified MSE error, $\mathcal{J}_{\text{MSE}} = p(t=1)\mathbb{E}[|\hat{\theta} - \theta|^2]$. Secondly, we freeze ν and train $f_\varepsilon, f_\mu, f_\eta, f_\sigma$ using just the second term of (6) in (8). Finally, we freeze σ, ν and train $f_\varepsilon, f_\mu, f_\eta, f_\rho$ by substituting \mathcal{J}_{NLL} with \mathcal{J}_{TD} .

D. Simulation Results without Hardware Impairments

We show the ISAC trade-off results in Fig. 2 (a) (SER vs. detection probability) and Fig. 2 (b) (SER vs. target RMSE). In the test stage, we established a fixed false alarm probability of $P_{\text{fa}} = 10^{-2}$ and computed the empirical value of P_{fa} during testing to obtain these results. Both figures indicate that the trade-off between radar and communication performance for the end-to-end learning approach based on different values of the hyper-parameter ω_r in (8) is close to the baseline. This confirms that ML approaches can perform as good as standard baselines for our particular scenario. The values of the hyper-parameters used in those simulations are $\omega_r \in \{0, 0.01, 0.014, 0.015, 0.03, 0.09, 0.15, 0.4, 0.6, 0.7, 1\}$.

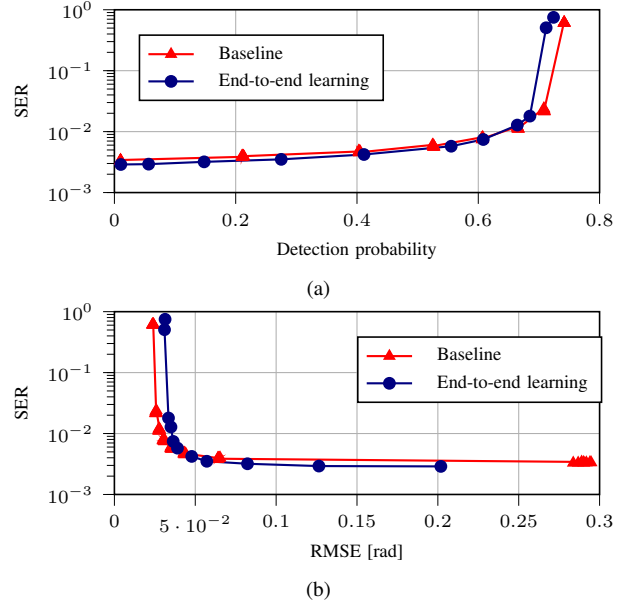


Fig. 2: Results (without hardware impairments) for a fixed empirical false alarm probability of $P_{\text{fa}} = 10^{-2}$, $\text{SNR}_c = 20$ dB, and $\text{SNR}_r = 0$ dB.

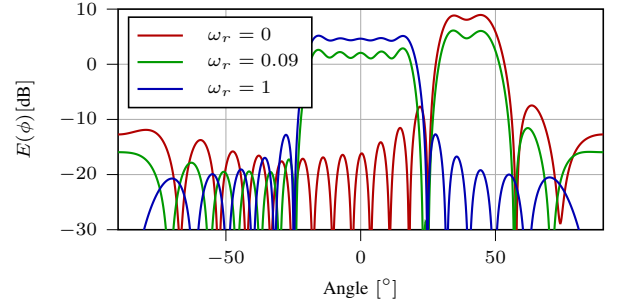


Fig. 3: Learned beampatterns (without hardware impairments) generated by the AE for different values of the hyper-parameter ω_r , where the communication receiver and the radar target reside, respectively, in the intervals $(30^\circ, 50^\circ)$ and $(-20^\circ, 20^\circ)$. The function $E(\phi) = |\mathbf{a}_{\text{tx}}(\phi)^\top \mathbf{y}|^2$ accounts for how much energy is transmitted in a certain direction.

We also observe a sharp degradation of communication performance when $\omega_r \rightarrow 1$, as the beamformer mainly illuminates the target and not the communication receiver, as seen in Fig. 3. Conversely, when $\omega_r \rightarrow 0$, the beamformer illuminates the communication receiver, leading to severe radar performance degradation (i.e., low detection probability and high RMSE). Nevertheless, there is a ‘sweet spot’ around $\omega_r \approx 0.09$, where both radar and communication achieve good performance, as the resulting beampattern points towards both angular sectors at the same time. Finally, in Fig. 4, we assess the quality of the AoA uncertainty estimate $\sigma_{\hat{\theta}}$. The RMSE increases monotonically with $\sigma_{\hat{\theta}}$ as ω_r varies, though we slightly under-estimate the RMSE.

E. Simulation Results under Hardware Impairments

We now study the impact of a specific hardware impairment: the inter-element spacing, which up to now was assumed to be exactly $d = \lambda/2$. Following [47], we apply a Gaussian perturbation, so that the distance between the k -th and $(k+1)$ -th antenna elements is $d_k \sim_{\text{i.i.d.}} \mathcal{N}(\lambda/2, \sigma_x^2)$. We set

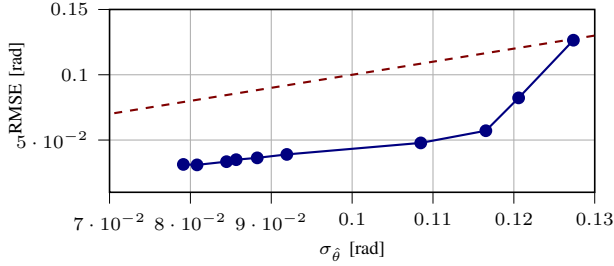


Fig. 4: Results (without hardware impairments) of the RMSE of the AoA against the associated standard deviation $\sigma_{\hat{\theta}}$ for $\omega_r \in \{0.01, 0.014, 0.015, 0.03, 0.09, 0.15, 0.4, 0.6, 0.7, 1\}$. The dashed line shows $\text{RMSE} = \sigma_{\hat{\theta}}$ as a reference.

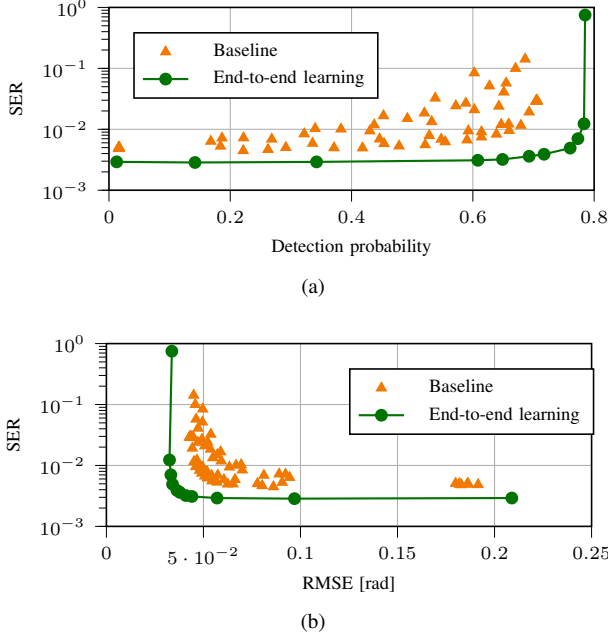


Fig. 5: Results (with hardware impairments) for a fixed empirical false alarm probability of $P_{\text{fa}} = 10^{-2}$, $\text{SNR}_c = 20$ dB, and $\text{SNR}_r = 0$ dB.

$\sigma_\lambda = \lambda/30$ and show the ISAC trade-off results for a single realization of d_k ($k = 0, \dots, K-2$) in Fig. 5. Note that the baseline assumes $d_k = \lambda/2, \forall k$. We observe that end-to-end learning can adapt to these hardware impairments, whereas standard model-based approach without a perfect model incurs significant performance penalties (despite the very small deviations from the nominal model). In this case the hyperparameter was selected to be $\omega_r \in \{0, 10^{-6}, 10^{-4}, 10^{-2}, 1.5 \cdot 10^{-2}, 0.03, 0.05, 0.15, 0.4, 0.9, 1\}$.

V. CONCLUSIONS

In this work, we have proposed a novel end-to-end AE approach for ISAC, and we have compared the AE performance with standard benchmarks for sensing and communications. Our results demonstrate that the trained AE performs close to the baseline. Moreover, we have shown the robustness of the proposed end-to-end learning approach to account for hardware impairments in the antenna array of the transmitter.

Among possible future works, some natural extensions to this study include: (i) incorporate multiple targets to the sensing environment, (ii) use a MIMO communication system, (iii)

provide ω_r to the AE input, (iv) learn across multiple angular ranges, and (v) make the channel more realistic towards 6G.

ACKNOWLEDGMENT

This work was supported, in part, by a grant from the Chalmers AI Research Center Consortium (CHAIR), by the European Commission through the H2020 project Hexa-X (Grant Agreement no. 101015956) and by the MSCA-IF grant 888913 (OTFS-RADCOM). The authors gratefully acknowledge the feedback from Juliano Pinto and Lennart Svensson.

APPENDIX A

RADAR DETECTION BENCHMARK

For the hypothesis testing problem where \mathcal{H}_0 and \mathcal{H}_1 denote the absence or presence of a target, the MAPRT corresponding to (1) can be written as [44]

$$\mathcal{L}(z_r) = \frac{\max_{\alpha, \theta, \mathbf{y}} p(\alpha, \theta, \mathbf{y}, \mathcal{H}_1 | z_r)}{p(\mathcal{H}_0 | z_r)} \underset{\mathcal{H}_0}{\overset{\mathcal{H}_1}{\gtrless}} \tilde{\eta}. \quad (12)$$

Notice that different from the Bayesian detector, we do not marginalize over α and θ in the MAPRT [44]. Applying the Bayes' theorem to (12) yields

$$\mathcal{L}(z_r) = \frac{\max_{\alpha, \theta, \mathbf{y}} p(z_r | \alpha, \theta, \mathbf{y}, \mathcal{H}_1) p(\alpha) p(\theta) p(\mathcal{H}_1)}{p(z_r | \mathcal{H}_0) p(\mathcal{H}_0)} \underset{\mathcal{H}_0}{\overset{\mathcal{H}_1}{\gtrless}} \tilde{\eta}. \quad (13)$$

Assuming $p(\mathcal{H}_0) = p(\mathcal{H}_1) = 1/2$ and taking the logarithm in (13), we obtain

$$\mathcal{L}^{\log}(z_r) = \frac{\|z_r\|^2}{N_0} - \min_{\alpha, \theta \in [\theta_{\min}, \theta_{\max}], \|\mathbf{y}\|^2 = E_{\text{tx}}} \left\{ \frac{\|z_r - \alpha \mathbf{a}_{\text{rx}}(\theta) \mathbf{a}_{\text{tx}}^\top(\theta) \mathbf{y}\|^2}{N_0} + \frac{|\alpha|^2}{\sigma^2} \right\} \underset{\mathcal{H}_0}{\overset{\mathcal{H}_1}{\gtrless}} \eta, \quad (14)$$

where $\mathcal{L}^{\log}(z_r) \triangleq \log \mathcal{L}(z_r)$, $\eta \triangleq \log \tilde{\eta} + \log(\theta_{\max} - \theta_{\min}) + \log(\pi \sigma^2)$, and the equality constraint on the transmit power is enforced to remove the ambiguity in estimating the channel gain α . The optimal α in (14) can be computed for given θ and \mathbf{y} as

$$\hat{\alpha} = \frac{\mathbf{y}^H \mathbf{a}_{\text{tx}}^*(\theta) \mathbf{a}_{\text{rx}}^H(\theta) z_r}{\|\mathbf{a}_{\text{rx}}(\theta) \mathbf{a}_{\text{tx}}^\top(\theta) \mathbf{y}\|^2 + \frac{N_0}{\sigma^2}} = \frac{\mathbf{y}^H \mathbf{a}_{\text{tx}}^*(\theta) \mathbf{a}_{\text{rx}}^H(\theta) z_r}{K |\mathbf{a}_{\text{tx}}^\top(\theta) \mathbf{y}|^2 + \frac{N_0}{\sigma^2}}. \quad (15)$$

Plugging (15) back into (14) yields (after some algebraic manipulations)

$$\mathcal{L}^{\log}(z_r) = \max_{\substack{\theta \in [\theta_{\min}, \theta_{\max}] \\ \|\mathbf{y}\|^2 = E_{\text{tx}}}} \frac{|\mathbf{a}_{\text{tx}}^\top(\theta) \mathbf{y}|^2 |\mathbf{a}_{\text{rx}}^H(\theta) z_r|^2}{N_0 \left(K |\mathbf{a}_{\text{tx}}^\top(\theta) \mathbf{y}|^2 + \frac{N_0}{\sigma^2} \right)} \underset{\mathcal{H}_0}{\overset{\mathcal{H}_1}{\gtrless}} \eta. \quad (16)$$

From (16), we can express the optimal \mathbf{y} as a function of θ as

$$\hat{\mathbf{y}} = \sqrt{\frac{E_{\text{tx}}}{K}} \frac{\mathbf{a}_{\text{tx}}^*(\theta) \mathbf{a}_{\text{rx}}^H(\theta) z_r}{|\mathbf{a}_{\text{rx}}^H(\theta) z_r|}. \quad (17)$$

Since $|\mathbf{a}_{\text{rx}}^\top(\theta)\hat{\mathbf{y}}|^2 = E_{\text{rx}}K$, inserting (17) into (16) yields the final detection test

$$|\mathbf{a}_{\text{rx}}^H(\hat{\theta})\mathbf{z}|^2 \underset{\mathcal{H}_0}{\overset{\mathcal{H}_1}{\geq}} \bar{\eta} \quad (18)$$

for some threshold $\bar{\eta}$ set to ensure a given false alarm probability, where $\hat{\theta} \triangleq \arg \max_{\theta \in [\theta_{\min}, \theta_{\max}]} |\mathbf{a}_{\text{rx}}^H(\theta)\mathbf{z}|^2$.

REFERENCES

- [1] H. Tataria *et al.*, “6G wireless systems: Vision, requirements, challenges, insights, and opportunities,” *Proc. IEEE*, Mar. 2021.
- [2] M. Matthaiou *et al.*, “The road to 6G: Ten physical layer challenges for communications engineers,” *IEEE Commun. Mag.*, vol. 59, no. 1, pp. 64–69, Feb. 2021.
- [3] W. Saad *et al.*, “A vision of 6G wireless systems: Applications, trends, technologies, and open research problems,” *IEEE Netw.*, vol. 34, no. 3, pp. 134–142, Oct. 2019.
- [4] S. M. Patole *et al.*, “Automotive radars: A review of signal processing techniques,” *IEEE Signal Process. Mag.*, vol. 34, no. 2, pp. 22–35, Mar. 2017.
- [5] A. R. Chiriyath *et al.*, “Radar-communications convergence: Coexistence, cooperation, and co-design,” *IEEE Trans. Cogn. Commun. Netw.*, vol. 3, no. 1, pp. 1–12, Feb. 2017.
- [6] D. K. P. Tan *et al.*, “Integrated sensing and communication in 6G: Motivations, use cases, requirements, challenges and future directions,” in *Proc. Int. Online Symp. Joint Commun. & Sens.* IEEE, Mar. 2021, pp. 1–6.
- [7] F. Liu *et al.*, “Integrated sensing and communications: Towards dual-functional wireless networks for 6G and beyond,” *arXiv preprint arXiv:2108.07165*, 2021.
- [8] M. L. Rahman *et al.*, “Enabling joint communication and radio sensing in mobile networks—a survey,” *arXiv preprint arXiv:2006.07559*, Jan. 2021.
- [9] H. Wymeersch *et al.*, “Integration of communication and sensing in 6G: a joint industrial and academic perspective,” *IEEE PIMRC Workshops*, Sept. 2021.
- [10] R. M. Mealey, “A method for calculating error probabilities in a radar communication system,” *IEEE Trans. Space Electron. Telemetry*, vol. 9, no. 2, pp. 37–42, Jun. 1963.
- [11] C. Sturm *et al.*, “Waveform design and signal processing aspects for fusion of wireless communications and radar sensing,” *Proc. IEEE*, vol. 99, no. 7, pp. 1236–1259, May 2011.
- [12] S. Sen, “Adaptive OFDM radar for target detection and tracking,” *Washington Univ. in St. Louis*, 2010. [Online]. Available: <https://doi.org/10.7936/K7JQ0Z3C>
- [13] L. Han *et al.*, “24-GHz integrated radio and radar system capable of time-agile wireless communication and sensing,” *IEEE Trans. Microw. Theory Techn.*, vol. 60, no. 3, pp. 619–631, Jan. 2012.
- [14] P. Kumari *et al.*, “Adaptive and fast combined waveform-beamforming design for mmWave automotive joint communication-radar,” *IEEE J. Sel. Topics in Signal Process.*, vol. 15, no. 4, pp. 996–1012, Apr. 2021.
- [15] C. Aydogdu *et al.*, “RadChat: Spectrum sharing for automotive radar interference mitigation,” *IEEE Trans. Intell. Transp. Syst.*, vol. 22, no. 1, pp. 416–429, Dec. 2019.
- [16] F. Liu *et al.*, “MU-MIMO communications with MIMO radar: From coexistence to joint transmission,” *IEEE Trans. Wireless Commun.*, vol. 17, no. 4, pp. 2755–2770, Feb. 2018.
- [17] C. B. Barneto *et al.*, “Beamformer design and optimization for full-duplex joint communication and sensing at mm-Waves,” *arXiv preprint arXiv:2109.05932*, Sep. 2021.
- [18] M. Braun, “OFDM radar algorithms in mobile communication networks,” *Karlsruher Inst. für Technol.*, 2014.
- [19] A. Hassani *et al.*, “Signaling strategies for dual-function radar communications: An overview,” *IEEE Aerosp. Electron. Syst. Mag.*, vol. 31, no. 10, pp. 36–45, Nov. 2016.
- [20] W. Scheibhofer *et al.*, “Method to embed a data-link on FMCW chirps for communication between cooperative 77-GHz radar stations,” in *Eur. Radar Conf.* IEEE, Dec. 2015, pp. 181–184.
- [21] L. Chen *et al.*, “Joint radar-communication transmission: A generalized pareto optimization framework,” *IEEE Trans. Signal Process.*, vol. 69, pp. 2752–2765, May 2021.
- [22] S. D. Liyanarachchi *et al.*, “Joint multi-user communication and MIMO radar through full-duplex hybrid beamforming,” in *Proc. Int. Online Symp. Joint Commun. & Sens.* IEEE, Mar. 2021, pp. 1–5.
- [23] S. H. Dokhanchi *et al.*, “Adaptive waveform design for automotive joint radar-communication systems,” *IEEE Trans. Veh. Technol.*, vol. 70, no. 5, pp. 4273–4290, Apr. 2021.
- [24] J. Johnston *et al.*, “MIMO OFDM dual-function radar-communication under error rate and beampattern constraints,” *arXiv preprint arXiv:2108.10555*, Aug. 2021.
- [25] F. Liu *et al.*, “Toward dual-functional radar-communication systems: Optimal waveform design,” *IEEE Trans. Signal Process.*, vol. 66, no. 16, pp. 4264–4279, Jun. 2018.
- [26] —, “Cramér-Rao bound optimization for joint radar-communication design,” *arXiv preprint arXiv:2101.12530*, Jan. 2021.
- [27] C. Liu *et al.*, “Learning-based predictive beamforming for integrated sensing and communication in vehicular networks,” *arXiv preprint arXiv:2108.11540*, Aug. 2021.
- [28] J. A. Zhang *et al.*, “Multibeam for joint communication and radar sensing using steerable analog antenna arrays,” *IEEE Trans. Veh. Technol.*, vol. 68, no. 1, pp. 671–685, Nov. 2018.
- [29] M. F. Keskin *et al.*, “Limited feedforward waveform design for OFDM dual-functional radar-communications,” *IEEE Trans. Signal Process.*, vol. 69, pp. 2955–2970, Apr. 2021.
- [30] O. Simeone, “A very brief introduction to machine learning with applications to communication systems,” *IEEE Trans. Cogn. Commun. Netw.*, vol. 4, no. 4, pp. 648–664, Nov. 2018.
- [31] P. Lang *et al.*, “A comprehensive survey of machine learning applied to radar signal processing,” *arXiv preprint arXiv:2009.13702*, Sep. 2020.
- [32] T. O’Shea *et al.*, “An introduction to deep learning for the physical layer,” *IEEE Trans. Cogn. Commun. Netw.*, vol. 3, no. 4, pp. 563–575, Oct. 2017.
- [33] F. A. Aoudia *et al.*, “Waveform learning for next-generation wireless communication systems,” *arXiv preprint arXiv:2109.00998*, Sep. 2021.
- [34] S. Cammerer *et al.*, “Trainable communication systems: Concepts and prototype,” *IEEE Trans. Commun.*, vol. 68, no. 9, pp. 5489–5503, Jun. 2020.
- [35] C. Zou *et al.*, “Channel autoencoder for wireless communication: State of the art, challenges, and trends,” *IEEE Commun. Mag.*, vol. 59, no. 5, pp. 136–142, Jun. 2021.
- [36] J. Song *et al.*, “Learning physical-layer communication with quantized feedback,” *IEEE Trans. Commun.*, vol. 68, no. 1, pp. 645–653, Nov. 2019.
- [37] W. Jiang *et al.*, “End-to-end learning of waveform generation and detection for radar systems,” in *Proc. Asilomar Conf. Signals, Syst. and Comput.* IEEE, Mar. 2019, pp. 1672–1676.
- [38] —, “Joint design of radar waveform and detector via end-to-end learning with waveform constraints,” *IEEE Trans. Aerosp. Electron. Syst.*, Feb. 2021.
- [39] J. Fuchs *et al.*, “Automotive radar interference mitigation using a convolutional autoencoder,” in *Proc. Int. Radar Conf.* IEEE, Jun. 2020, pp. 315–320.
- [40] Z. Qin *et al.*, “Deep learning in physical layer communications,” *IEEE Wireless Commun.*, vol. 26, no. 2, pp. 93–99, Mar. 2019.
- [41] J. Pinto *et al.*, “An uncertainty-aware performance measure for multi-object tracking,” *IEEE Signal Process. Lett.*, vol. 28, pp. 1689–1693, Aug. 2021.
- [42] A. Alkhatib *et al.*, “Channel estimation and hybrid precoding for millimeter wave cellular systems,” *IEEE J. Sel. Topics Signal Process.*, vol. 8, no. 5, pp. 831–846, Jul. 2014.
- [43] J. Tranter *et al.*, “Fast unit-modulus least squares with applications in beamforming,” *IEEE Trans. Signal Process.*, vol. 65, no. 11, pp. 2875–2887, Feb. 2017.
- [44] S. Guruacharya *et al.*, “MAP ratio test detector for radar system,” *IEEE Trans. Signal Process.*, vol. 69, pp. 573–588, Dec. 2021.
- [45] E. Conte *et al.*, “GLRT-based adaptive detection algorithms for range-spread targets,” *IEEE Trans. Signal Process.*, vol. 49, no. 7, pp. 1336–1348, Jul. 2001.
- [46] D. P. Kingma *et al.*, “Adam: A method for stochastic optimization,” *arXiv preprint arXiv:1412.6980*, Jan. 2017.
- [47] T. Yassine *et al.*, “mpNet: variable depth unfolded neural network for massive MIMO channel estimation,” *arXiv preprint arXiv:2008.04088*, Aug. 2020.